Chemical Synthesis of β-Ga2O3 Microrods on Silicon and Its Dependence on the Gallium Nitrate Concentration

Guislain Hector, Estelle Appert, Eirini Sarigiannidou, Elea Matheret, Herve Roussel, Odette Chaix-Pluchery, Vincent Consonni

Chemical Synthesis of β-Ga_2O_3 Microrods on Silicon and Its Dependence on the Gallium Nitrate Concentration

Guislain Hector,[1] Estelle Appert,[1] Eirini Sarigiannidou,[1] Eléa Matheret,[1] Hervé Roussel,[1] Odette Chaix-Pluchery,[1] and Vincent Consonni.[1*]

[1]*Univ. Grenoble Alpes, CNRS, Grenoble INP, LMGP, F-38000 Grenoble, France*

***Corresponding Author:**

Vincent Consonni

LMGP, Grenoble INP – Minatec, 3 parvis Louis Néel – CS 50257 – 38016 Grenoble cedex 1

Tel : (+33) 456529358

vincent.consonni@grenoble-inp.fr

ABSTRACT

β-Ga_2O_3 microrods have received in the last years an increasing interest for their integration into solar blind / UV photodetectors and gas sensors. However, their synthesis using a low temperature chemical route in aqueous solution is still under development and the physicochemical processes at work have not been elucidated yet. Here, we develop a double-step process involving the growth of α-GaOOH microrods on silicon using chemical bath deposition and their further structural conversion into β-Ga_2O_3 microrods by post-deposition thermal treatment. It is revealed that the concentration of gallium nitrate has a drastic effect to tune the morphology, dimensions (i.e. diameter and length), and density of α-GaOOH microrods over a broad range, governing in turn the morphological properties of β-Ga_2O_3 microrods. The physicochemical processes in aqueous solution are investigated by thermodynamic computations yielding speciation diagrams of Ga(III) species and theoretical solubility plots of GaOOH(s). In particular, the qualitative evolution of the morphological properties of α-GaOOH microrods with the concentration of gallium nitrate is found to be correlated with the supersaturation in the bath and discussed in the light of the standard nucleation and growth theory. Interestingly, the structural conversion following the thermal treatment at 900 °C in air results in the formation of pure β-Ga_2O_3 microrods without any residual minor phases and with tunable morphology and improved structural ordering. These findings reporting a double-step process to form high quality pure β-Ga_2O_3 microrods on silicon open many perspectives for their integration onto a large number of substrates for solar blind / UV photo-detection and gas sensing.

INTRODUCTION

As an ultra-wide band gap semiconductor with a long-term stability, a high melting point of 1800 °C, a high breakdown electric field of 8 MV/cm and a high electron mobility around 300 cm^2/V s, gallium oxide (Ga_2O_3) has received over the last years an increasing interest in the fields of solar blind / ultra-violet photo-detection, gas sensing, power electronics, and field-effect transistors.[1,2] A striking particularity of Ga_2O_3 is related to the existence of five polymorphs, namely the corundum (α), monoclinic (β), defective spinel (γ), and orthorhombic (ε) phases with the δ phase being a type of the orthorhombic phase. Under ambient pressure and temperature conditions, the monoclinic β-phase of Ga_2O_3 represents the most stable crystal structure and has attracted much attention.

As high aspect ratio structures at respective nano- and micro-scale dimensions, Ga_2O_3 wires and rods have emerged as building blocks for many of these applications. The growth of Ga_2O_3 wires and rods has typically been achieved in the framework of the vapor-liquid-solid / vapor-solid approaches using metal catalysts.[3] A vast number of vapor phase deposition techniques has been used such as chemical vapor deposition, metal-organic chemical vapor deposition, vapor phase epitaxy, physical evaporation, arc discharge, laser ablation, and thermal oxidation of metal Ga.[4,5,6,7,8,9,10] In the present techniques, the implementation of vacuum in the reactor is typically required along with a high growth temperature. In contrast, the solution deposition techniques as low-cost, low temperature, and easily implemented processes offer a wide range of assets, but has not extensively been developed so far.

Over the last decades, a broad variety of solution deposition techniques has been developed including sol-gel process, hydrothermal synthesis, and chemical bath deposition (CBD).[1,2] Among them, the CBD process using water as solvent and working at low temperature (< 100 °C) and atmospheric pressure is particularly attractive and appears as a cost-effective, safe, and ecofriendly process. This chemical synthesis route has been used to obtain nano and micro-particles of Ga_2O_3 following the calcination of pre-deposited gallium(III) oxide-hydroxide (GaOOH) particles. Sato *et al.*[11] first explored the synthesis of gallium(III) hydroxide ($Ga(OH)_3$) particles by CBD using different alkali species and pH. They obtained amorphous $Ga(OH)_3$ particles for each alkali species and pH, and revealed their influence on the ageing time required for the crystallization of the orthorhombic α-GaOOH phase. Tas *et al.*[12] studied

the influence of the homogeneous decomposition of urea on the morphological and structural properties of GaOOH and Ga_2O_3 particles using forced hydrolysis. They described two different morphologies depending on the presence of urea or not, and the formation of porosity in particles due to the dehydration of the GaOOH phase. This study has led to several investigations tuning the morphology of GaOOH particles by CBD using the homogeneous deposition in the bath. Zhao *et al.*[13] obtained micro-sized GaOOH rods using gallium nitrate ($Ga(NO_3)_3$), polyethylene oxide (PEO) and cetyltrimethylammoniumbromide (CTAB). Qian *et al.*[14] achieved the uniform synthesis of spindle GaOOH particles using gallium chloride as the gallium chemical precursor and ammonia or ethylenediamine as alkali species. Krehula *et al.*[15] synthesised particles using tetramethylammonium hydroxide (TMAH). Later on, Huang *et al.*[16] described the influence of the ionic strength on the morphological and structural properties of GaOOH particles by varying the sodium nitrate ($NaNO_3$) over $Ga(NO_3)_3$ concentration ratio.

The CBD process has also been used for the formation of GaOOH particles using the heterogeneous deposition on substrates. In 2005, Fujihara *et al.*[17] studied the heterogeneous deposition of GaOOH particles on different oxide and fluoride substrates, including quartz, TiO_2 (both anatase and rutile phases), SnO_2, commercial SnO_2:F, β-Ga_2O_3, MgO, MgF_2, ZnO, CeO_2, and $BaTiO_3$. The substrates were placed in a reactor containing an aqueous solution of $Ga(NO_3)_3$ kept at 60 °C for 1 to 48 hours. It was shown that the heterogeneous nucleation and growth of GaOOH particles are promoted on TiO_2, MgO, and SnO_2/SnO_2:F substrates. This study has led to several investigations using SnO_2 as a typical substrate to create GaOOH rod arrays. For instance, Lin *et al.*[18] achieved the formation of β-Ga_2O_3 nanorod arrays using a hydrothermal synthesis for carbon oxide detection. Silicon substrates were first coated with a 50 nm-thick SnO_2 layer that was subsequently incubated in a reactor containing an aqueous solution of $Ga(NO_3)_3$ kept at 150 °C for 12 hours. They obtained arrays of vertically aligned GaOOH nanorods with a mean diameter and length of 100-300 nm and 2 µm, respectively. The substrates were eventually annealed at 1000 °C for 4 hours to obtain β-Ga_2O_3 nanorod arrays. Liang *et al.*[19] obtained nanorod arrays on SnO_2:F using CBD process in static and dynamic conditions. $Ga(NO_3)_3$ was used as the gallium chemical precursor and urea as the alkali species. In both static and dynamic conditions, the temperature

was kept at 95 °C and the deposition occurred for 24 hours. In dynamic conditions, the chemical precursor solution was injected through the reactor at 1 mL/min. The dynamic conditions led to the increase in the length of rods by a factor of four as compared to static conditions. It was further stated that the growth mechanism of GaOOH nanorod arrays could be driven by screw dislocations.

As an alternative substrate for device integration using Ga_2O_3 rods, the widely used silicon has a great potential. However, only few investigations have reported the formation of Ga_2O_3 rods on silicon substrates by the hydrothermal synthesis and CBD processes. Also, the physicochemical processes at work in the bath and the nucleation and growth mechanisms involved on silicon are still open to a large extent. Sinha *et al.*[19] obtained long spindle-like GaOOH particles on silicon. The process involved a home-made gallium chemical precursor fabricated from metallic gallium and hydrochloric acid and ethylene glycol as the co-solvent with water. The silicon substrate was sealed in an autoclave containing the solution and put at 200 °C for 4 - 12 hours. They showed the strong influence of ethylene glycol on the morphological evolution of GaOOH particles starting from rhombus-shaped rods after 4 hours of reaction to long needle-like rods after 12 hours of reaction. Later on, Zhang *et al.*[21] achieved the synthesis of GaOOH microrod arrays on silicon with a two-step hydrothermal process. The silicon substrate was first immerged in alcoholic solution (25/75 %v EtOH/water) containing $Ga(NO_3)_3$ kept at 100 °C for 30 min. Then, it was put into an autoclave system with a pure aqueous solution of $Ga(NO_3)_3$ and kept at 150 °C for 12 hours. They obtained a uniform array with rhombus-shaped GaOOH rods. They also compared this method with a single-step hydrothermal process involving a pure aqueous solution of $Ga(NO_3)_3$ and another two-step process without ethanol. However, the arrays were less vertical, less dense, and less uniform than the process with ethanol. This was explained by the fact that ethanol reduces the contact angle between the solution and substrate, favoring in turn the heterogeneous nucleation of GaOOH particles on silicon.

In this work, we develop the formation of β-Ga_2O_3 microrods on silicon by using a double-step process involving CBD and post-deposition thermal treatment. Microsized α-GaOOH rods are grown by CBD on silicon and converted into β-Ga_2O_3 microrods by thermal treatment in air. The structural conversion from α-GaOOH to pure β-Ga_2O_3 phase is characterized by x-ray diffraction (XRD),

transmission-electron microscopy (TEM), and Raman spectroscopy. Additionally, the effect of the $Ga(NO_3)_3$ concentration ranging from 15 to 100 mM on the morphology of α-GaOOH microrods is shown along with the physicochemical processes at work in the bath by using thermodynamic computations yielding speciation diagram of Ga(III) species and theoretical solubility plots. The nucleation and growth mechanisms of α-GaOOH microrods on silicon are further discussed qualitatively in the light of the standard nucleation and growth theory.

METHODS

Deposition Techniques. Ga_2O_3 microrods were grown on silicon by a double-step process involving CBD and post-deposition thermal treatment. Prior to the process, the Si (001) substrates were cleaned with acetone and isopropanol under sonicating bath to remove organic pollutants. GaOOH microrods were initially grown by CBD using an aqueous solution containing gallium nitrate hydrate ($Ga(NO_3)_3.xH_2O$, 99,9%, Sigma-Aldrich) with a concentration varying in the range of 15 – 100 mM. All chemical precursor solutions were prepared by dissolving the given amount of $Ga(NO_3)_3$ in ultrapure water. To ensure the complete dissolution of the chemical precursor, the solutions were placed on a hot plate and magnetically stirred at 70 °C for 12 hours. The Si(001) substrates were then placed face down in a sealed reactor containing the given chemical precursor solution located in a regular oven kept at 70 °C for 24 hours. At the end of the CBD process, the Si(001) substrates were washed with distilled water and dried under nitrogen flow. The solution was also filtrated using a Büchner method to collect the homogeneous deposit in the bath. Eventually, GaOOH microrods were annealed in air in a tubular furnace kept at 900 °C for 1 hour.

Characterization Techniques. The morphological properties of GaOOH and Ga_2O_3 microrods were investigated with a FEI Quanta 250 field-emission scanning electron microscopy (FESEM) instrument. XRD patterns were collected with a Bruker D8 Advance diffractometer using Cu $K_{\alpha 1}$ radiation according to the Bragg−Brentano configuration. The crystallographic analysis was carried out with TOPAS software provided by Bruker. Raman spectroscopy was performed by using a Horiba/Jobin Yvon Labram spectrometer equipped with a liquid nitrogen-cooled CCD detector. The 488

nm line of an Ar^+ laser with a power on the sample surface close to 1 mW was focused to a spot size smaller than 1 μm^2 using a 100 times long working distance objective. The spectra were calibrated using a silicon reference sample at room temperature by fixing the theoretical position of the silicon Raman line to 520.7 cm^{-1}. Cross-section TEM lamella were prepared using the semi-automated polishing tripod technique with the MultiPrepTM system (Allied High Tech Prodcuts, Inc.). For the final polishing, a GATAN PIPS II system was used. TEM and HRTEM images were recorded with a JEOL JEM 2010 LaB_6 microscope operating at 200 kV with a 0.19 nm point-to-point resolution.

Thermodynamic Computations. Thermodynamic calculations were performed with Visual MINTEQ software for the determination of the speciation diagrams of Ga(III) species as well as the theoretical solubility plots of GaOOH at 70 °C for each growth condition (*i.e.*, with varying $Ga(NO_3)_3$ concentration). The formation of hydroxide complexes between the single metallic cations in aqueous solution (Ga^{3+} ions), denoted as M^{x+}, and the single possible ligand (HO^-), denoted as L, occurs according to the general reactions: $nM^{x+} + iL \leftrightarrow M_nL_i^{x+}$, where $M_nL_i^{x+}$ is the complex considered, i is the coordination number, and x is the cation charge. The related stability constants β_i^L associated with each reaction are given by: $\beta_i^L = \frac{[M_nL_i^{nx+}]}{[M^{x+}]^n[L]^i}$. These constants were taken at 25 °C from NIST for Ga(III) species and are presented in **Table S1** in Supporting Information. The constants at 70 °C were deduced from Van't Hoff relation. The calculation of the theoretical solubility plots for each growth condition was achieved by taking into account GaOOH(s) and $Ga(OH)_3$ (am), using the solubility constants K_s presented in **Table S2** in Supporting Information.

RESULTS AND DISCUSSION

Morphology and Dimensions of Microrods. Typical top-view and cross-sectional view FESEM images of microstructures grown by CBD with a $Ga(NO_3)_3$ concentration of 15, 25, and 50 mM are shown in **Figure 1**. The evolution of their dimensions, aspect ratio, and apparent density as a function of the $Ga(NO_3)_3$ concentration is presented in **Figure 2**.

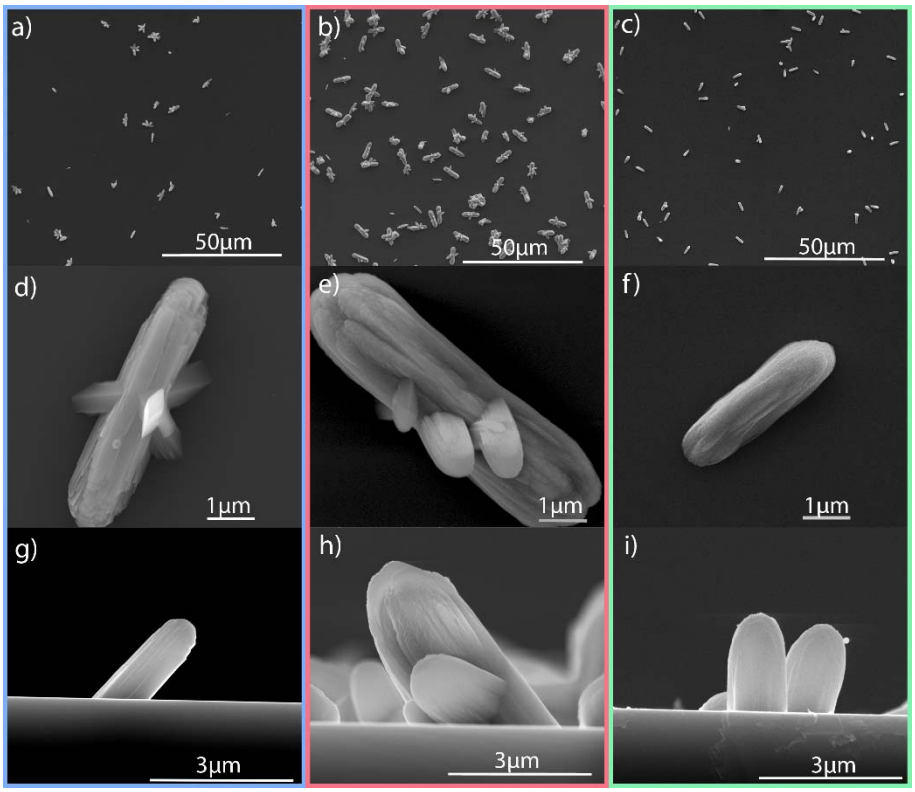

Figure 1. Typical top-view FESEM images with a (a-c) low and (d-f) high magnification as well as (g-i) cross-sectional view FESEM images of GaOOH microrods grown with a $Ga(NO_3)_3$ concentration of (a,d,g) 15, (b,e,h) 25, and (c,f,i) 50 mM corresponding to the so-called plate-layered rod (PLR), round-plate rod (RPR), and round-rod (RR) morphologies, respectively.

Depending on the $Ga(NO_3)_3$ concentration, three types of rod-like microstructures (*i.e.*, microrods) with different morphologies are typically formed directly on silicon. The microrods thus grow according to a heterogeneous nucleation process. No chemical treatment is required to activate the present process. For a $Ga(NO_3)_3$ concentration of 15 mM, the so-called plate-layered rods (PLR) with a hierarchical structure are formed, as presented in **Figures 1a** and **1d**. The PLRs are composed of the stack of thin, sharp plates with the occurrence of few secondary nucleation places at their base. They have a morphology that is fairly similar to the accordion-like shape where the prismatic plates are stacked, as reported by Krehula *et al.*[15] For a $Ga(NO_3)_3$ concentration of 25 mM, the PLRs are transformed into the so-called round-plate rods (RPR), also presenting a hierarchical architecture with few secondary nucleation places at their base, as seen in **Figures 1b** and **1e**. However, the stack of the apparent layers is not evident and the microstructure of RPRs is more textured than the microstructure of PLRs. For the

larger $Ga(NO_3)_3$ concentrations of 50, 75 and 100 mM, the RPRs are transformed into the so-called round-rods (RR), as revealed in **Figures 1c** and **1f**. The RRs present a shape that is fairly close to the RPR morphology, but no secondary nucleation takes place at their base. The RRs get thinner and smaller as the $Ga(NO_3)_3$ concentration is increased and could be associated with the "zeppelin",[12] "rice" or "spindle-like shape" widely reported in the literature.[12,15,16,21,22,23] The present RR morphology is commonly obtained as the precipitation occurs in acidic medium. Overall, the three types of microrods grown on silicon are significantly tilted with respect to the normal to the substrate surface, as depicted in **Figures 1g-i**. The tilt angle varies over a broad range of 0 to 90 ° for all the microrods, but both PLRs and RPRs appear to be more inclined. The dimensions including the mean diameter and length of microrods are shown in **Figure 2a**. The biggest microrods corresponding to the PLRs and RPRs are grown for $Ga(NO_3)_3$ concentrations of 15 mM and 25 mM, for which the mean diameter and length reach 1.20 and 5 µm as well as 2 and 7.25 µm, respectively. Then, as the $Ga(NO_3)_3$ concentration is further increased from 50 to 100 mM, RRs are formed with a mean diameter and length decreasing from 1.15 and 4 µm to a saturation plateau around the values of 0.65 and 2 µm, respectively. Correlatively, the mean aspect ratio of microrods continuously decreases as the $Ga(NO_3)_3$ concentration is increased from 15 to 100 mM, and ends up saturating around the value of 3.30 for the highest concentration. The number density of microrods is presented in **Figure 2b**. Regardless of the $Ga(NO_3)_3$ concentration, the number density of microrods is low and much smaller than the typical number density obtained in the CBD process of other oxide nanowires. It is increased from about 0.25 to 1 rod/100µm² and thus multiplied by a factor of 4 as the $Ga(NO_3)_3$ concentration is increased from 15 to 100 mM. The deposited volume of microrods as presented in **Figure 3** exhibits the same evolution as their dimensions with a maximum at a $Ga(NO_3)_3$ concentration of 25 mM, indicating that its variation is mainly influenced by the behavior of the dimensions.

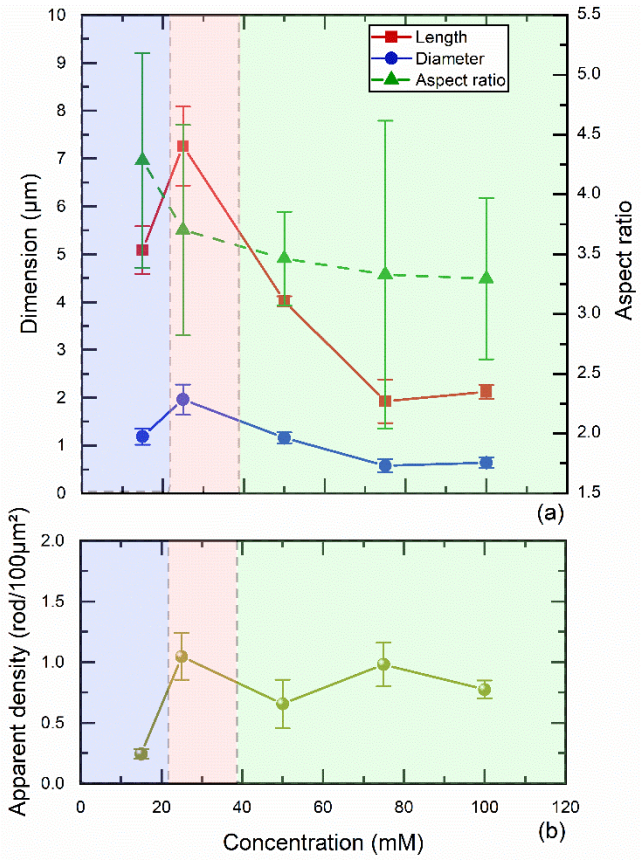

Figure 2. (a) Evolution of the mean dimensions (i.e. length and diameter) and aspect ratio of GaOOH microrods as a function of the $Ga(NO_3)_3$ concentration. (b) Evolution of the number density of GaOOH microrods as a function of the $Ga(NO_3)_3$ concentration. The blue, red, and green area denote the formation domains of the so-called plate-layered rod (PLR), round-plate rod (RPR), and round-rod (RR) morphologies, respectively.

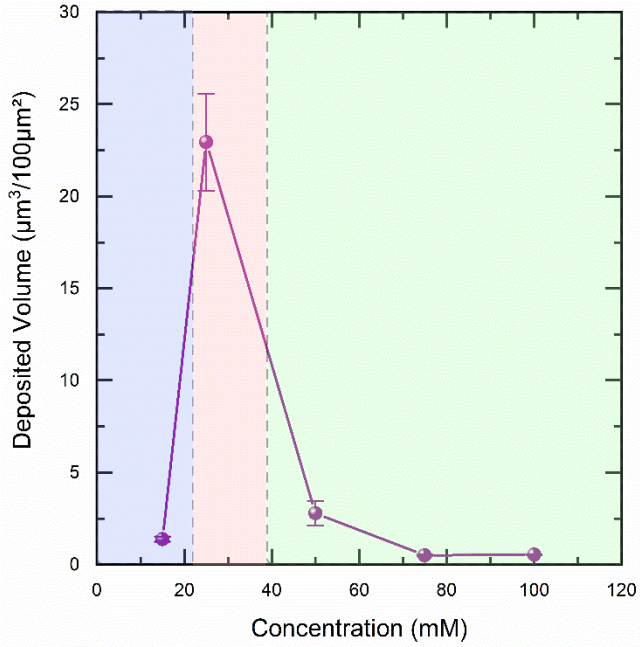

Figure 3. Evolution of the deposited volume of GaOOH microrods as a function of the $Ga(NO_3)_3$ concentration. The blue, red, and green area denote the formation domains of the so-called plate-layered rod (PLR), round-plate rod (RPR), and round-rod (RR) morphologies, respectively.

Crystallographic Structure of Microrods. The crystallographic structure of as-grown microrods is reported in the following when using a CBD process with a $Ga(NO_3)_3$ concentration of 25 mM resulting in the RPR morphology, but the analysis is similar for the other $Ga(NO_3)_3$ concentrations and resulting PLR/RR morphologies. SEM-EDS spectra of microrods collected before and after thermal treatment at 900 °C for 1 hour in air are presented in **Figure 4**.

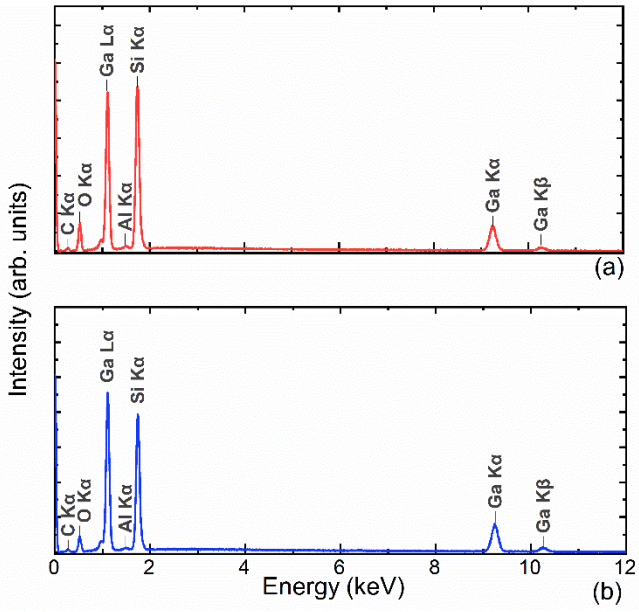

Figure 4. FESEM-EDS spectra of microrods (a) before and (b) after thermal treatment at 900 °C for 1 hour in air.

The Ga L_α, K_α, and K_β lines at 1.098, 9.252, and 10.264 keV along with the O K_α line at 0.525 keV occur in both EDS spectra of microrods before and after thermal treatment. The Si K_α line at 1.740 keV is also detected and originates from the silicon substrate. It should be noted here that both Al and C K_α lines are due to the nature of detector in the SEM system and to the use of carbon tape, respectively. Overall, the FESEM-EDS spectra thus reveal that the microrods before and after thermal treatment are composed of gallium and oxygen chemical elements.

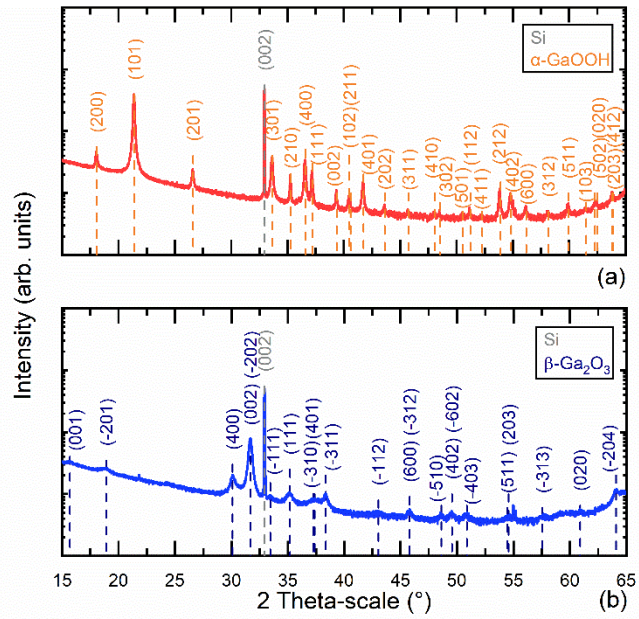

Figure 5. XRD patterns of microrods (a) before and (b) after thermal treatment at 900 °C for 1 hour in air.

XRD patterns of microrods collected before and after thermal treatment at 900 °C for 1 hour in air are presented in **Figure 5**. The experimental XRD pattern of as-grown microrods seen in **Figure 5a** very well matches the α-GaOOH orthorhombic phase belonging to the *Pnma* space group and corresponding to the calculated ICDD 04-010-9861 file with the following lattice parameters: a = 9.79 Å, b = 2.97 Å, and c = 4.51 Å. However, a small deviation between the theoretical and experimental XRD patterns occurs here. In order to solve all the lattice parameters, a complete XRD pattern was computed with the TOPAS software from Bruker. The computed XRD pattern is in very good agreement with the experimental XRD pattern with the following inferred lattice parameters: a = 9.81 Å, b = 2.97 Å, and c = 4.57 Å. The preferential growth direction and the degree of preferred orientation σ were further estimated by determining the texture coefficient C_{hkl} of each (hkl) plane as follows:

$$C_{hkl} = \frac{\frac{I_{hkl}}{I_{0,hkl}}}{\frac{1}{N}\cdot\sum_{N}\frac{I_{hkl}}{I_{0,hkl}}} \text{ and } \sigma = \frac{\sqrt{\sum_{N}\left(C_{hkl}-1\right)^2}}{\sqrt{N}} \qquad (1)$$

where N is the number of diffraction peaks involved, I_{hkl} is the experimental intensity of the diffraction peak, and $I_{0,hkl}$ is the intensity of the diffraction peak given by the ICDD 04-010-9861 file. In the case of a randomly oriented growth, the texture coefficient and degree of preferred orientation should be equal to 1 and 0, respectively. In the case of a perfectly oriented growth (along hkl), the texture coefficient and degree of preferred orientation should reach $(C_{hkl})_{max}$ = N (for hkl plane) and $(C_{hkl})_{min}$ = 0 (for other planes) as well as $\sigma_{max} = (N-1)^{1/2}$, respectively. The texture coefficients and degree of preferred orientation of α-GaOOH microrods deduced from N = 10 diffraction peaks are summarized in **Table S3** in Supporting Information. It appears that the preferential growth direction corresponds to the direction normal to the (101) plane with a related texture coefficient around 2.86. However, the degree of preferred orientation of 0.74 is fairly low as compared to σ_{max} = 3, indicating that α-GaOOH microrods are poorly oriented. The experimental XRD pattern of microrods after thermal treatment seen in **Figure 5b** does

not show any diffraction peaks attributed to the α-GaOOH orthorhombic phase. Instead, the experimental XRD pattern very well matches the monoclinic β-Ga_2O_3 phase belonging to the C_{2h}^3 (*C2/m*) space group and corresponding to the ICDD 00-041-1103 file with the following lattice parameters: a = 12.20 Å, b = 3.04 Å, c = 5.80 Å, α,γ = 90°, and β = 103.64°. Also, no diffraction peaks attributed to the rhombohedral α-Ga_2O_3 phase corresponding to the ICDD 00-006-0503 file occur. This indicates that the structural conversion process from α-GaOOH microrods to β-Ga_2O_3 microrods has been completed following the thermal treatment at 900 °C for 1 hour in air. Following the same XRD analysis as reported in **Table S3** in Supporting Information, it appears that the preferential growth direction of β-Ga_2O_3 microrods corresponds to the direction normal to the (001) plane with a related texture coefficient of 3.67. A high overall texture coefficient of 2.59 in the directions normal to the (-202) and (002) planes is also obtained, but the corresponding diffraction peaks overlap and the individual contributions of each diffraction peak cannot be readily unraveled. It is also worth noticing that the degree of preferred orientation of β-Ga_2O_3 microrods significantly increases to a value of 1.11, which is greater than the corresponding value for α-GaOOH microrods with the RPR morphology. A strengthening of the structural ordering is thus concomitant with the conversion process from α-GaOOH to β-Ga_2O_3 microrods.

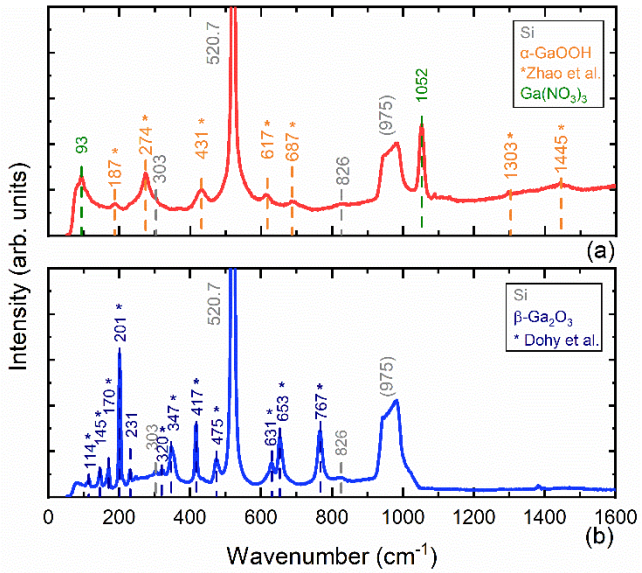

Figure 6. Raman spectra of microrods collected (a) before and (b) after thermal treatment at 900 °C for 1 hour in air. The star icons in (a) and (b) refer to the investigations of Zhao *et al.* and Dohy *et al.*, respectively.

Raman spectra of microrods collected before and after thermal treatment at 900 °C for 1 hour in air are presented in **Figure 6**. In both spectra, the intense Raman line at 520.7 cm^{-1} along with the weak and second-order lines at 303, 826, and around 975 cm^{-1} originate from the silicon substrate. The Raman lines at 187, 274, 431, 617, 687, 1303, and 1445 cm^{-1} in **Figure 6a** are characteristic of the orthorhombic structure of α-GaOOH as reported by Zhao *et al.*[24] They confirm the formation of α-GaOOH microrods before thermal treatment, which is in very good agreement with the corresponding XRD patterns. According to Zhao *et al.*,[24,25] only the lines at 274, 431, 1303, and 1445 cm^{-1} are specific to the α-GaOOH phase. The two first ones are assigned to the O-Ga-O bending mode and symmetric stretching mode of the GaO_6 octahedra, respectively, while the last ones are not assigned. The other lines are common to the α-GaOOH and β-Ga_2O_3 phases and thus correspond to the same vibrations in both structures. By analogy with the β-Ga_2O_3 phase, the lines at 617 and 687 cm^{-1} are attributed to the O-Ga-O bending mode and symmetric stretching mode of the GaO_4 tetrahedra, respectively, and the one at 187 cm^{-1} to the libration and translations of tetrahedra-octahedra chains.[26] The weak and intense lines at 93 and 1052 cm^{-1}, respectively, could be due to gallium nitrate hydrate precursor residues ($Ga(NO_3)_3.8H_2O$).[27] The first one has not been assigned yet, while the other one is assigned to the NO_3^- (ν_1) stretching mode.
The Raman lines at 114, 145, 170, 201, 320, 347, 417, 475, 631, 653, and 767 cm^{-1} in **Figure 6b** are characteristic of the monoclinic structure of β-Ga_2O_3 [24,26,28] and confirm the formation of β-Ga_2O_3 microrods after thermal treatment. This is again in very good agreement with the corresponding XRD patterns. Additionally, no Raman signal coming from the α-GaOOH phase is detected either, indicating that the structural conversion process to β-Ga_2O_3 microrods has been completed. The β-Ga_2O_3 phase belongs to the C_{2h}^3 (C2/m) space group.[29] The unit cell contains two formula units and is composed of GaO_4 tetrahedral and GaO_6 octahedral chains aligned along the *b*-axis. [28,30] According to the factor group analysis at the Γ point, 15 Raman and 12 infrared active modes are expected in the β-Ga_2O_3 vibrational spectrum.[26,30] The lines at 114 (A_g+B_g), 145 (B_g), 170 (A_g), and 201 cm^{-1} (A_g) are related to lattice modes

(*i.e.*, libration and translations of tetrahedra-octahedra chains).[26,30] The lines at 320 (A_g), 347 (A_g), 417 (A_g), and 475 cm^{-1} (A_g+B_g) are assigned to deformation modes of GaO_6 octahedra.[24] Eventually, the line at 631 cm^{-1} (A_g) is ascribed to O-Ga-O bending modes of tetrahedral GaO_4 units, and those at 653 (A_g+B_g) and 767 cm^{-1} (A_g) to symmetric stretching modes of GaO_4 units.[24] It should be noted that the β-Ga_2O_3 Raman modes related to our microrods have positions very close to those found with bulk β-Ga_2O_3.[24,26,30] Additionally, the line at 1052 cm^{-1} has completely vanished after thermal treatment, indicating the decomposition of the NO_3^- groups that is expected to occur below 300°C.[31] This supports the complete decomposition of gallium nitrate hydrate precursor residues ($Ga(NO_3)_3.8H_2O$) after thermal treatment. The nature of the remaining line at 231 cm^{-1} has not been clarified yet. It corresponds neither to the α-Ga_2O_3 phase,[32] nor to the γ-Ga_2O_3 [33] or ε-Ga_2O_3 phases.[34] As a result, the presence of these allotropic phases in the microrods after thermal treatment is excluded. Instead, the unassigned line could originate from impurities or defects in the centre of microrods, as suggested by Gao *et al.*[35]

Microstructure of Microrods. TEM images of microrods collected before and after thermal treatment at 900 °C for 1 hour in air are presented in **Figure 7**. The microrods have the RPR morphology obtained when using the CBD process with a $Ga(NO_3)_3$ concentration of 25 mM.

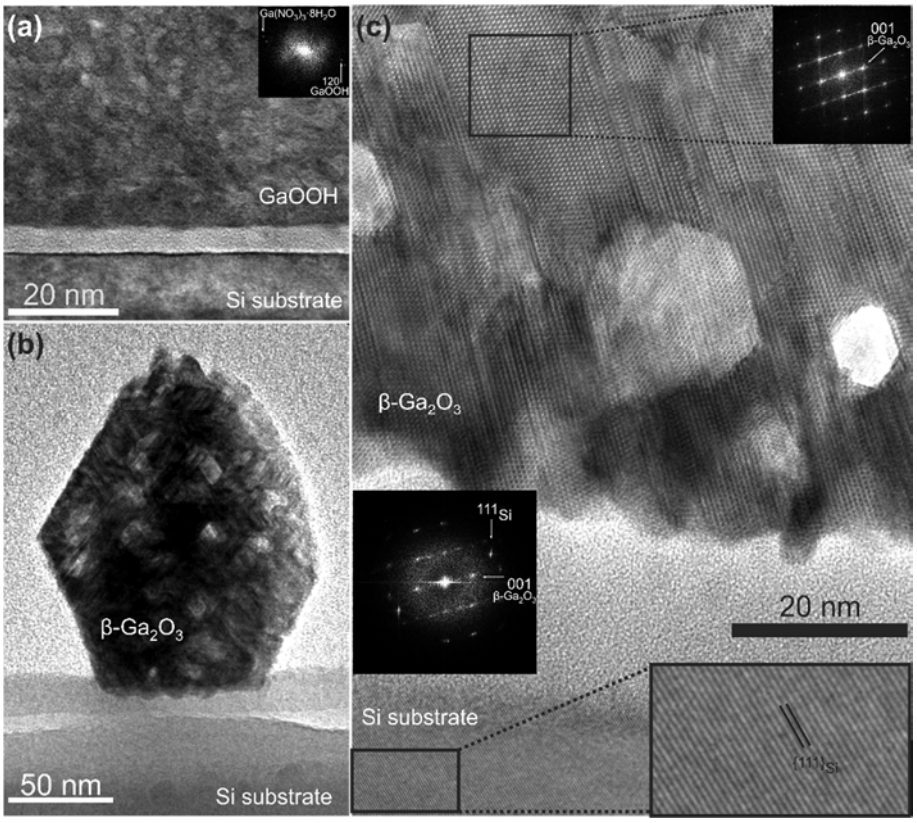

Figure 7. (a) Low-magnification TEM image of the interfacial region of an as-grown GaOOH microrod on silicon. The FFT of a GaOOH area is given as an inset. (b) Cross-sectional TEM image of a porous β-Ga_2O_3 microrod after thermal treatment on silicon. (c) HRTEM image of the interfacial region of a β-Ga_2O_3 microrod after thermal treatment on silicon. The (111) planes of silicon are denoted in a magnified inset. The FFT of the interfacial area and of the β-Ga_2O_3 area along the [010] zone axis are shown in the respective insets.

Before thermal treatment, the formation of α-GaOOH microrods with the orthorhombic structure occurs on the native SiO_x amorphous layer with a thickness of 4.5 ± 0.3 nm, as shown in **Figure 7a**. The Fourier-filtered enhancement of the GaOOH area confirms the presence of gallium nitrate hydrate precursor residues ($Ga(NO_3)_3.8H_2O$). The microrod further exhibits a high density of small porous domains with a mean size of less than 5 nm. After thermal treatment, the formation of β-Ga_2O_3 microrods with the monoclinic structure is shown in **Figure 7b**. The SiO_x amorphous layer has been thickened during thermal treatment to reach a mean value of 22 ± 7 nm. The microrod exhibits a reduced density of porous domains, but their size is four times larger on average. Also, a number of extended defects has been formed in the structure, as revealed in **Figure 7c**. Interestingly, the 001 reflection of the β-Ga_2O_3 microrod is misaligned by an angle of approximately 17.5 ° with respect to the (111) planes of silicon. The thickening of the native SiO_x amorphous layer along with the fairly small misalignment of β-Ga_2O_3 microrods indicate that their crystallization during thermal treatment is assisted by diffusion and is strongly affected by the silicon (111) surface underneath.

Physicochemical processes during the CBD. The physicochemical processes governing the CBD of oxide nano/microstructures following the heterogeneous nucleation on a dedicated substrate have extensively been investigated in titanium dioxide (TiO_2)[36,37] and zinc oxide (ZnO).[38,39] The driving force for the crystallization process of nano/microstructures is given by the difference between the chemical potential of the metallic species in solution and the chemical potential of the solid phase $\Delta\mu$ as follows:

$$\Delta\mu = k_b\, T \ln (a/a^*) \qquad (2)$$

where T is the growth temperature, k_b is the Boltzmann constant, a and a^* are the mean ionic activity of the solution at any time and at equilibrium, respectively. Basically, the supersaturation ratio (S_R) is defined as: $S_R = a / a^*$. Following a couple of approximations on the nature of solution, S_R can be expressed as: $S_R = C / C^*$ where C and C^* are the concentrations of the solution at any time and at equilibrium involving metallic species, respectively. In addition, the absolute supersaturation S_A is given by:[40] $S_A = C - C^*$. It is well-known that the physicochemical processes in the CBD involve a competition between the heterogeneous (*i.e.* on the substrate) and homogeneous (*i.e.* inside the bulk solution) nucleation, which strongly depends on the magnitude of S_R. Usually, when the value of S_R is large, the homogeneous nucleation process is predominant. In contrast, when the value of S_R is small, the heterogeneous nucleation process dominates. The control of the magnitude of S_R is basically one of the key parameters for the CBD process. A common strategy has consisted in adding urea or hexamethylenetetramine (HMTA) in aqueous solution, which progressively releases OH^- ions and hence maintains a fairly small constant S_R. This strategy has been widely used for growing ZnO nanostructures[41,42] and also developed by several groups to obtain GaOOH microrods directly deposited on the substrate.[17,19,43,44] However, Tas *et al.* showed the advantage of using a simple forced hydrolysis to obtain GaOOH microrods by CBD without any chemical additives and at low temperature and standard pressure, opening the way for developing a green chemistry process.

In order to understand in more details the physicochemical processes driving the formation of α-GaOOH microrods, both speciation diagram of Ga(III) species and theoretical solubility plots were computed using Visual MINTEQ software. The following Ga(III) species and solid phases were taken into account in the analysis: Ga^{3+}, $GaOH^{2+}$,$Ga(OH)_2^+$,$Ga(OH)_4^-$, $Ga(OH)_3$(am) and GaOOH(s). The speciation diagram of the different Ga(III) species at 70 °C for a $Ga(NO_3)_3$ concentration of 25 mM is shown in **Figure 8**. The curves were deduced from the equilibrium calculation for each pH value at 70 °C, starting from pH = 1 to pH = 12 with a 0.001 incremental step. It appears that only Ga(III) species and GaOOH solid phase occur at equilibrium. No $Ga(OH)_3$(am) species are formed over the considered range of pH. Three main ionic species are found: Ga^{3+}, $GaOH^{2+}$, and $Ga(OH)_4^-$ ions. The Ga(III) cationic species including Ga^{3+} and $GaOH^{2+}$ ions are predominant for a pH value smaller than 1.9. Their concentration dramatically decreases in the pH range of 1.9 – 9 owing to the precipitation of GaOOH(s).

Then, the dissolution of the GaOOH precipitate starts at a pH value of about 9. The $Ga(OH)_4^-$ anionic species dominate for a pH value larger than 9. Its concentration increases to reach the initial $Ga(NO_3)_3$ concentration of 25 mM at a pH value of 12. Overall, the speciation diagram shows a very large amount of Ga^{3+} ions in the present CBD conditions lying in the pH range of 1.72 – 1.96. This suggests a forced hydrolysis[12] reaction involving Ga^{3+} ions and water as the main chemical reaction:

$$Ga^{3+} + 2H_2O \Rightarrow GaOOH + 3H^+ \quad (3)$$

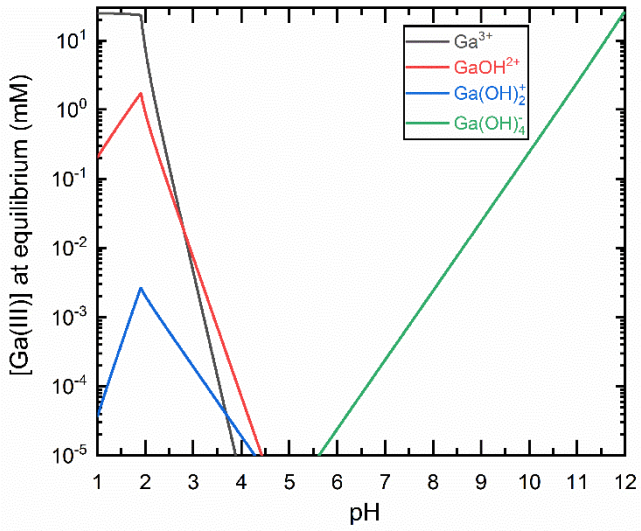

Figure 8. Speciation diagram of Ga(III) species at 70 °C as a function of the pH for a $Ga(NO_3)_3$ concentration of 25 mM.

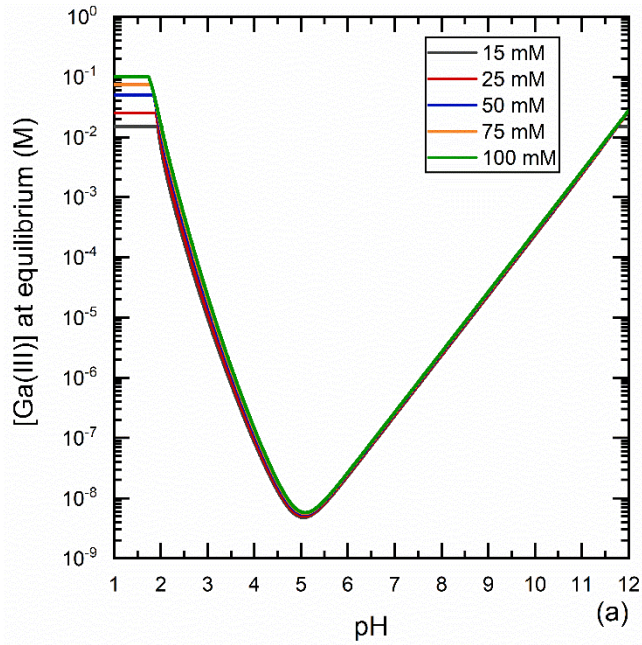

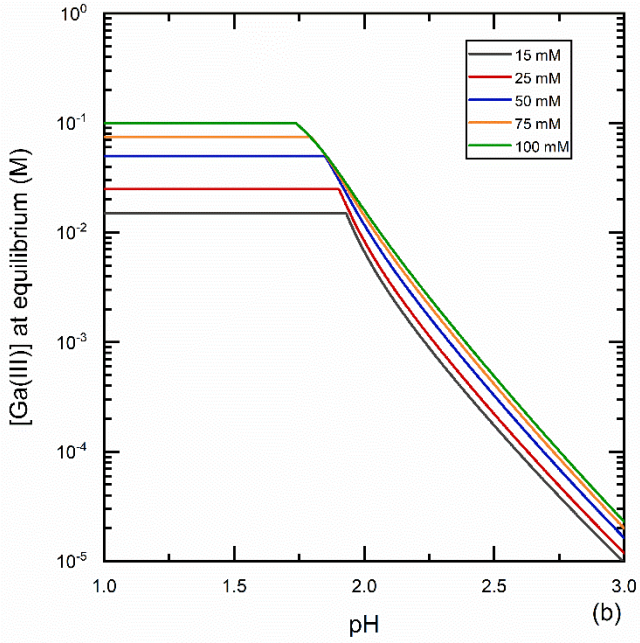

Figure 9. Theoretical solubility plots of Ga(III) species at 70 °C as a function of the pH for a $Ga(NO_3)_3$ concentration of 15, 25, 50, 75, and 100 mM.

The theoretical solubility plots of Ga(III) species at 70 °C are presented in **Figure 9a** with a zoom-in in the area of interest in **Figure 9b**. The values of the pH at equilibrium, concentration of Ga(III) species at equilibrium C^*, S_A, and S_R are presented in **Table 1.**

$Ga(NO_3)_3$ concentration (mM)	pH at equilibrium	[Ga(III)] at equilibrium (C^*) (mM)	Absolute supersaturation (S_A) (mM)	Supersaturation ratio (S_R)
15	1.958	10.66	4.34	1.41
25	1.921	20.16	4.84	1.24
50	1.863	44.40	5.60	1.13
75	1.808	68.76	6.24	1.09
100	1.752	93.10	6.90	1.07

Table 1. pH at equilibrium, concentration of Ga(III) species at equilibrium C^*, S_A, and S_R for a $Ga(NO_3)_3$ concentration of 15, 25, 50, 75 and 100 mM.

From these theoretical data using thermodynamic computations, the nucleation and growth mechanisms of α-GaOOH microrods can be drawn using standard nucleation and growth theory. In this approach, the dimensions (*i.e.*, diameter and length) of α-GaOOH microrods are related to the crystal growth rate G whereas their density is dependent upon the heterogeneous nucleation rate J. Interestingly, G and J are respectively dependent upon S_A and S_R as follows: [40,45]

$$G \propto S_A \quad (4)$$

$$J \propto S_R \exp[-B/\ln^2(S_R)] \quad (5)$$

where B is a thermodynamic parameter independent upon S_R. As shown in **Table 1**, S_A significantly increases from 4.34 to 6.90 as the $Ga(NO_3)_3$ concentration is increased from 15 to 100 mM. As a consequence, G also increases in that $Ga(NO_3)_3$ concentration range. Correlatively, the mean diameter and length of α-GaOOH microrods drastically increase from 15 to 25 mM, as shown in **Figure 2a**. However, the mean diameter and length of α-GaOOH microrods strongly decrease eventually from 25 to 100 mM. This can be explained by the kinetic aspect of the reaction. The delay between the establishment of the supersaturation in solution and the formation of the first critical nuclei is characterized by the induction time t_i that is expressed by:[40]

$$t_i = 1/(JV) \quad (6)$$

where V is the volume of the system. t_i is thus related to S_R through J. As the $Ga(NO_3)_3$ concentration is further increased from 25 to 100 mM, the significant reduction of S_R leads to a strong increase in the delay before the formation of the first critical nuclei and thus to a highly prolonged t_i. As a result, the effective growth time $t_{effective}$ required for elongating the α-GaOOH microrods is strongly reduced as the $Ga(NO_3)_3$ concentration is increased from 25 to 100 mM, resulting in a decrease in the mean diameter and length of α-GaOOH microrods. Owing to the dependences of G and t_i on S_A and S_R, the increase in S_A cannot compensate for the decrease in S_R. Additionally, the dependence of J on S_R also plays a significant role on the number density of α-GaOOH microrods. In this investigation, S_R is close to a value of 1 and thus the number density of α-GaOOH microrods is very low, regardless of the $Ga(NO_3)_3$ concentration. The number density of α-GaOOH microrods is however even smaller for a $Ga(NO_3)_3$ concentration of 15 mM and then relatively stable in the range of 25 - 100 mM, as shown in **Figure 2b**. According to the collected mass plot of homogeneous precipitate in **Figure S1** (see Supporting Information), the homogeneous nucleation is much more pronounced for the $Ga(NO_3)_3$ concentration of 15 mM as S_R is much larger. It is believed that Ga^{3+} ions are globally less available for the heterogeneous nucleation on the substrate in that case, decreasing in turn J and hence lowering the number density of

α-GaOOH microrods. It is also likely that the number of nucleation sites on the silicon surface is fairly limited.

Ga_2O_3 as well as other M_2O_3 (Al_2O_3, Fe_2O_3 …) oxides are polymorphic compounds. Roy *et al.*[46] and Playford *et al.*[47] described and characterized four Ga_2O_3 allotropic phases (α-,β-,γ-,ε-Ga_2O_3) , one additional potential allotropic phase (δ-Ga_2O_3) and a transient orthorhombic phase κ-Ga_2O_3. However, only α-Ga_2O_3 and β-Ga_2O_3 are expected to be formed by CBD at low temperature and without the use of surfactants or co-solvent. In the second step of the CBD process, it is possible to preferentially obtain α-Ga_2O_3 or β-Ga_2O_3 by tuning the conditions of the thermal treatment.[46,47,48] As reported by Fujirama *et al.*,[17] the α-GaOOH microrods annealed at 900 °C for 1 hour in air form Ga_2O_3 microstructures. A high temperature thermal treatment in air typically leads to the structural conversion process of the α-GaOOH phase into the pure β-Ga_2O_3 phase following the main dehydration reaction:

$$2GaOOH \Rightarrow Ga_2O_3 + H_2O \quad (7)$$

The annealing temperature of 900 °C used here to crystallize the β phase of Ga_2O_3 could be lowered by optimizing that second step of the CBD process. Lower annealing temperatures during thermal treatment can reduce the thermal budget and increase the potential of integration of these microrods. The structural conversion process is accompanied by a reduction of the porosity rate in the microrods as shown in **Figure 7**, but does not affect their morphology and dimensions. As a result, the optimization of the morphological and structural properties of α-GaOOH microrods during the first step of the CBD process represents an efficient way to form high quality β-Ga_2O_3 microrods following the second step of thermal treatment. The physicochemical processes at work to form α-GaOOH microrods by CBD are complex and characterized by a significant competition between the homogeneous and heterogeneous depositions, a low supersaturation level, and a prolonged induction time to name a few. The integration of β-Ga_2O_3 microrods onto silicon open numerous perspectives for the development of innovative devices in the fields of solar blind / UV photo-detection and gas sensing, where efficient light trapping phenomena for boosting the optical absorption and large surface area for enhancing the chemical reactions are highly desired, respectively.

CONCLUSION

In summary, we have developed a double-step process to form pure β-Ga_2O_3 microrods with different morphologies on silicon. The process involves the growth of α-GaOOH microrods on silicon by CBD and their further structural conversion into β-Ga_2O_3 microrods by post-deposition thermal treatment. The $Ga(NO_3)_3$ concentration has been found to drastically affect the morphology, dimensions (i.e. diameter and length), and density of α-GaOOH microrods by CBD. This represents an efficient way to tune the resulting morphological properties of β-Ga_2O_3 microrods over a broad range following the post-deposition thermal treatment. The physicochemical processes in aqueous solution have been investigated in detail by thermodynamic computations yielding the predominant Ga(III) species and the supersaturation levels as well as their dependence on the $Ga(NO_3)_3$ concentration. The qualitative evolution of the morphological properties of α-GaOOH microrods with the $Ga(NO_3)_3$ concentration has further been correlated with the supersaturation level in the bath and discussed in the light of the standard nucleation and growth theory. Interestingly, the structural conversion following the thermal treatment at 900 °C in air leads the formation of pure β-Ga_2O_3 microrods without any residual minor phases and with tunable morphology and improved structural ordering. The density of porous domains in the β-Ga_2O_3 microrods is also decreased during the structural conversion, but with an increase in their size. These findings report a double-step process to form high quality pure β-Ga_2O_3 microrods on silicon and emphasize the physicochemical processes at work. They open many perspectives for the integration of β-Ga_2O_3 microrods onto a large number of substrates for solar blind / UV photo-detection and gas sensing.

ASSOCIATED CONTENT

Possible chemical reactions in aqueous solution and related equilibrium constants K at 25 °C, considering the Ga-OH chemical system (Table S1); solubility constants K_s at 25 °C for the solid phases of gallium-based compounds (Table S2); texture coefficients C_{hkl} and degree of preferred orientation σ for the main diffraction peaks, along with their intensities for α-GaOOH and β-Ga_2O_3 microrods (Table S3); collected mass plot of homogeneous precipitate as a function of the $Ga(NO_3)_3$ concentration (Figure S1).

ACKNOWLEDGEMENTS

The authors acknowledge the financial support from the French Research National Agency through the project DOSETTE (ANR-17-CE24-0004). G.H. held a doctoral fellowship from the DOSETTE project. The authors further acknowledge the facilities, and the scientific and technical assistance of the CMTC characterization platform of Grenoble INP, which is supported by the Centre of Excellence of Multifunctional Architectured Materials (LabEx CEMAM) under the contract ANR-10-LABX-44-01 funded by the "Investments for the Future" Program.

REFERENCES

(1) Pearton, S. J.; Yang, J.; Cary, P. H.; Ren, F.; Kim, J.; Tadjer, M. J.; Mastro, M. A. A Review of Ga_2O_3 Materials, Processing, and Devices. *Appl. Phys. Rev.* **2018**, *5* (1), 011301.

(2) Chen, X.; Ren, F.; Gu, S.; Ye, J. Review of Gallium-Oxide-Based Solar-Blind Ultraviolet Photodetectors. *Photonics Res.* **2019**, *7* (4), 381.

(3) Chang, P.-C.; Fan, Z.; Tseng, W.-Y.; Rajagopal, A.; Lu, J. G. β-Ga2O3 Nanowires: Synthesis, Characterization, and p-Channel Field-Effect Transistor. *Appl. Phys. Lett.* **2005**, *87* (22), 222102.

(4) Auer, E.; Lugstein, A.; Löffler, S.; Hyun, Y. J.; Brezna, W.; Bertagnolli, E.; Pongratz, P. Ultrafast VLS Growth of Epitaxial β- Ga_2O_3 Nanowires. *Nanotechnology* **2009**, *20* (43), 434017.

(5) Kim, N. H.; Kim, H. W.; Seoul, C.; Lee, C. Amorphous Gallium Oxide Nanowires Synthesized by Metalorganic Chemical Vapor Deposition. *Mater. Sci. Eng. B* **2004**, *111* (2–3), 131–134.

(6) Murakami, H.; Nomura, K.; Goto, K.; Sasaki, K.; Kawara, K.; Thieu, Q. T.; Togashi, R.; Kumagai, Y.; Higashiwaki, M.; Kuramata, A.; Yamakoshi, S.; Monemar, B.; Koukitu, A. Homoepitaxial Growth of β-Ga_2O_3 Layers by Halide Vapor Phase Epitaxy. *Appl. Phys. Express* **2015**, *8* (1), 015503.

(7) Zhang, H. Z.; Kong, Y. C.; Wang, Y. Z.; Du, X.; Bai, Z. G.; Wang, J. J.; Yu, D. P.; Ding, Y.; Hang, Q. L.; Feng, S. Q. Ga2O3 Nanowires Prepared by Physical Evaporation. *Solid State Commun.* **1999**, *109* (11), 677–682.

(8) Choi, Y. C.; Kim, W. S.; Park, Y. S.; Lee, S. M.; Bae, D. J.; Lee, Y. H.; Park, G.-S.; Choi, W. B.; Lee, N. S.; Kim, J. M. Catalytic Growth of β-Ga2O3 Nanowires by Arc Discharge. *Adv. Mater.* **2000**, *12* (10), 746–750.

(9) Hu, J. Q.; Li, Q.; Meng, X. M.; Lee, C. S.; Lee, S. T. Synthesis of β-Ga_2O_3 Nanowires by Laser Ablation. *J. Phys. Chem. B* **2002**, *106* (37), 9536–9539.

(10) Vanithakumari, S. C.; Nanda, K. K. A One-Step Method for the Growth of Ga_2O_3 -Nanorod-Based White-Light-Emitting Phosphors. *Adv. Mater.* **2009**, *21* (35), 3581–3584.

(11) Sato, T.; Nakamura, T. Studies of the Crystallisation of Gallium Hydroxide Precipitated from Hydrochloric Acid Solutions by Various Alkalis. *J. Chem. Technol. Biotechnol.* **2007**, *32* (3), 469–475.

(12) Taş, A. C.; Majewski, P. J.; Aldinger, F. Synthesis of Gallium Oxide Hydroxide Crystals in Aqueous Solutions with or without Urea and Their Calcination Behavior. *J. Am. Ceram. Soc.* **2002**, *85* (6), 1421–1429.

(13) Zhao, Y.; Frost, R. L.; Martens, W. N. Synthesis and Characterization of Gallium Oxide Nanostructures via a Soft-Chemistry Route. *J. Phys. Chem. C* **2007**, *111* (44), 16290–16299.

(14) Qian, H.-S.; Gunawan, P.; Zhang, Y.-X.; Lin, G.-F.; Zheng, J.-W.; Xu, R. Template-Free Synthesis of Highly Uniform α-GaOOH Spindles and Conversion to α-Ga_2O_3 and β-Ga_2O_3. *Cryst. Growth Des.* **2008**, *8* (4), 1282–1287.
(15) Krehula, S.; Ristić, M.; Kubuki, S.; Iida, Y.; Fabián, M.; Musić, S. The Formation and Microstructural Properties of Uniform α-GaOOH Particles and Their Calcination Products. *J. Alloys Compd.* **2015**, *620*, 217–227.
(16) Huang, E.; Li, J.; Wu, G.; Dai, W.; Guan, N.; Li, L. A Simple Synthesis of Ga_2O_3 and GaN Nanocrystals. *RSC Adv* **2017**, *7* (76), 47898–47903.
(17) Fujihara, S.; Shibata, Y.; Hosono, E. Chemical Deposition of Rodlike GaOOH and β-Ga[Sub 2]O[Sub 3] Films Using Simple Aqueous Solutions. *J. Electrochem. Soc.* **2005**, *152* (11), C764.
(18) Lin, H.-J.; Baltrus, J. P.; Gao, H.; Ding, Y.; Nam, C.-Y.; Ohodnicki, P.; Gao, P.-X. Perovskite Nanoparticle-Sensitized Ga_2O_3 Nanorod Arrays for CO Detection at High Temperature. *ACS Appl. Mater. Interfaces* **2016**, *8* (14), 8880–8887.
(19) Liang, H.; Meng, F.; Lamb, B. K.; Ding, Q.; Li, L.; Wang, Z.; Jin, S. Solution Growth of Screw Dislocation Driven α-GaOOH Nanorod Arrays and Their Conversion to Porous $ZnGa_2O_4$ Nanotubes. *Chem. Mater.* **2017**, *29* (17), 7278–7287.
(20) Sinha, G.; Pal, U.; Zaldivar, M. H.; Patra, A. Synthesis of *α* -GaO(OH) Nanorods and Their Optical Properties. *J. Nanosci. Nanotechnol.* **2010**, *10* (3), 1982–1988.
(21) Zhang, J.; Jiao, S.; Wan, Y.; Gao, S.; Wang, D.; Wang, J. A Well-Grown β-Ga_2O_3 Microrod Array Formed from GaOOH on a Si (100) Substrate and Growth Mechanism Study. *CrystEngComm* **2018**, *20* (30), 4329–4335.
(22) Li, G.; Peng, C.; Li, C.; Yang, P.; Hou, Z.; Fan, Y.; Cheng, Z.; Lin, J. Shape-Controllable Synthesis and Morphology-Dependent Luminescence Properties of GaOOH:Dy^{3+} and β-Ga_2O_3:Dy^{3+}. *Inorg. Chem.* **2010**, *49* (4), 1449–1457.
(23) Zhao, Y.; Frost, R. L.; Yang, J.; Martens, W. N. Size and Morphology Control of Gallium Oxide Hydroxide GaO(OH), Nano- to Micro-Sized Particles by Soft-Chemistry Route without Surfactant. *J. Phys. Chem. C* **2008**, *112* (10), 3568–3579.
(24) Zhao, Y.; Frost, R. L. Raman Spectroscopy and Characterisation of α-Gallium Oxyhydroxide and β-Gallium Oxide Nanorods. *J. Raman Spectrosc.* **2008**, *39* (10), 1494–1501.
(25) Zhao, Y.; Yang, J.; Frost, R. L. Raman Spectroscopy of the Transition of α-Gallium Oxyhydroxide to β-Gallium Oxide Nanorods. *J. Raman Spectrosc.* **2008**, *39* (10), 1327–1331.
(26) Dohy, D.; Lucazeau, G. Raman Spectra and Valence Force Field of Single-Crystalline J3 Ga,O,. *Jounal Solid State Chem.* **1982**, *45*, 180–192.
(27) Rudolph, W. W.; Pye, C. C.; Irmer, G. Study of Gallium(III) Nitrate Hydrate and Aqueous Solutions: Raman Spectroscopy Andab Initio Molecular Orbital Calculations of Gallium(III) Water Clusters. *J. Raman Spectrosc.* **2002**, *33* (3), 177–190.
(28) Onuma, T.; Fujioka, S.; Yamaguchi, T.; Itoh, Y.; Higashiwaki, M.; Sasaki, K.; Masui, T.; Honda, T. Polarized Raman Spectra in β-Ga2O3 Single Crystals. *J. Cryst. Growth* **2014**, *401*, 330–333.
(29) Geller, S. Crystal Structure of B-Ga_2O_3. *J. Chem. Phys.* **1960**, *33* (3), 676–684.
(30) Rao, R.; Rao, A. M.; Xu, B.; Dong, J.; Sharma, S.; Sunkara, M. K. Blueshifted Raman Scattering and Its Correlation with the [110] Growth Direction in Gallium Oxide Nanowires. *J. Appl. Phys.* **2005**, *98* (9), 094312.
(31) Małecka, B.; Lacz, A.; Drozdz, E.; Malecki, A. Thermal Decomposition of d-Metal Nitrates Supported on Alumina. *J. Therm. Anal. Calorim.* **2015**, *119*, 1053-1061.
(32) Machon, D.; McMillan, P. F.; Xu, B.; Dong, J. High-Pressure Study of the β -to- α Transition in Ga 2 O 3. *Phys. Rev. B* **2006**, *73* (9).
(33) Seshadri, H.; Cheralathan, M.; Sinha, P. K. Photocatalytic Performance of Combustion-Synthesized β and γ-Ga2O3 in the Degradation of 1,4-Dioxane in Aqueous Solution. *Res. Chem. Intermed.* **2013**, *39* (3), 991–1001.
(34) Kracht, M.; Karg, A.; Schörmann, J.; Weinhold, M.; Zink, D.; Michel, F.; Rohnke, M.; Schowalter, M.; Gerken, B.; Rosenauer, A.; Klar, P. J.; Janek, J.; Eickhoff, M. Tin-Assisted Synthesis of ε − Ga 2 O 3 by Molecular Beam Epitaxy. *Phys. Rev. Appl.* **2017**, *8* (5).

(35) Gao, Y. H.; Bando, Y.; Sato, T.; Zhang, Y. F.; Gao, X. Q. Synthesis, Raman Scattering and Defects of β-Ga2O3 Nanorods. *Appl. Phys. Lett.* **2002**, *81* (12), 2267–2269.
(36) More, A. M., Gujar, T. P.; Gunjakar, J. L.; Lokhande, C. D.; Joo, O. H. Growth of TiO_2 Nanorods by Chemical Bath Deposition Method. *Appl. Surf. Sci.* **2008**, *255* (5), 2682-2687.
(37) Pawar, S. M.; Pawar, B. S.; Kim, J. H.; Joo, O. S.; Lokhande, C. D. Recent Status of Chemical Bath Deposited Metal Chalcogenide and Metal Oxide Thin Films. *Curr. Appl. Phys.* **2011**, *11* (2), 117-161.
(38) Vayssieres, L.; Keis, K.; Lindquist, S.-E.; Hagfeldt, A. Purpose-Built Anisotropic Metal Oxide Material: 3D Highly Oriented Microrod Array of ZnO. *J. Phys. Chem. B* **2001**, *105* (17), 3350–3352.
(39) Govender, K.; Boyle, D. S.; Kenway, P. B.; O'Brien, P. Understanding the Factors That Govern the Deposition and Morphology of Thin Films of ZnO from Aqueous Solution. *J Mater Chem* **2004**, *14* (16), 2575–2591.
(40) Kashchiev, D.; van Rosmalen, G. M. Review: Nucleation in Solutions Revisited. *Cryst. Res. Technol.* **2003**, *38* (78), 555–574.
(41) Strano, V.; Urso, R. G.; Scuderi, M.; Iwu, K. O.; Simone, F.; Ciliberto, E.; Spinella, C.; Mirabella, S. Double Role of HMTA in ZnO Nanorods Grown by Chemical Bath Deposition. *J. Phys. Chem. C* **2014**, *118* (48), 28189–28195.
(42) Parize, R.; Garnier, J.; Chaix-Pluchery, O.; Verrier, C.; Appert, E.; Consonni, V. Effects of Hexamethylenetetramine on the Nucleation and Radial Growth of ZnO Nanowires by Chemical Bath Deposition. *J. Phys. Chem. C* **2016**, *120* (9), 5242–5250.
(43) Yeh, C.-Y.; Zhao, Y.-M.; Li, H.; Yu, F.-P.; Zhang, S.; Wuu, D.-S. Growth and Photocatalytic Properties of Gallium Oxide Films Using Chemical Bath Deposition. *Crystals* **2019**, *9* (11), 564.
(44) Zhang, J.; Jiao, S.; Wang, D.; Ni, S.; Gao, S.; Wang, J. Solar-Blind Ultraviolet Photodetection of an α-Ga_2O_3 Nanorod Array Based on Photoelectrochemical Self-Powered Detectors with a Simple, Newly-Designed Structure. *J. Mater. Chem. C* **2019**, *7* (23), 6867–6871.
(45) Roelands, C. P. M.; ter Horst, J. H.; Kramer, H. J. M.; Jansens, P. J. Analysis of Nucleation Rate Measurements in Precipitation Processes. *Cryst. Growth Des.* **2006**, *6* (6), 1380–1392.
(46) Roy, R.; Hill, V. G.; Osborn, E. F. Polymorphism of Ga_2O_3 and the System Ga_2O_3 —H_2O. *J. Am. Chem. Soc.* **1952**, *74* (3), 719–722.
(47) Playford, H. Y.; Hannon, A. C.; Barney, E. R.; Walton, R. I. Structures of Uncharacterised Polymorphs of Gallium Oxide from Total Neutron Diffraction. *Chem. - Eur. J.* **2013**, *19* (8), 2803–2813.
(48) Wang, X.; Xu, Q.; Fan, F.; Wang, X.; Li, M.; Feng, Z.; Li, C. Study of the Phase Transformation of Single Particles of Ga_2O_3 by UV-Raman Spectroscopy and High-Resolution TEM. *Chem. - Asian J.* **2013**, *8* (9), 2189–2195.